Detector Design for the ALPHA-g Time Projection Chamber and Laser Imaging for Antihydrogen Cooling and Spectroscopy

Matt Grant

Engineering Physics Student

University of British Columbia

Dr. Makoto Fujiwara and Dr. Mario Michan

Supervisors

TRIUMF and CERN

(Dated: September 22, 2015)

ACKNOWLEDGEMENTS

I would first like to sincerely thank Dr. Makoto Fujiwara. I am very grateful and honored to have had such a mentor while still an undergraduate student. It was under his guidance where I was able to develop into the type of student to be considered for an IPP Summer Fellowship in the first place. My appreciation also extends to Dr. Mario Michan. Dr. Michan was a true pleasure to work under and another excellent mentor. I would also like to thank The Institute of Particle Physics for giving me this unforgettable opportunity. Finally, I want to thank everyone in the ALPHA collaboration for reasons too numerous to list. I cannot imagine a more beneficial way to spend my summer.

CONTENTS

1. BACKGROUND AND INTRODUCTION

The current laws of physics tell us that equal amounts of matter and antimatter were created in the big bang. Given symmetric properties between the two, as demanded by the standard model, all particles should have annihilated very shortly afterwards. However, one in ten billion matter particles survived to make up our known universe. On the other hand, antimatter is relatively non-existent. This implies *asymmetric* properties and therefore illustrates one of the forefront enigmas challenging modern particle physicists.

The ALPHA collaboration seeks fundamental asymmetries between H (H) and antihydrogen ($\bar{H}$) in hopes of finding anything to explain this mystery and correct the present laws of physics. The ALPHA-g experiment will probe the gravitational reaction of antimatter. This will be performed with a vertical atom trap (see Figure 1). If the $\bar{H}$ are of low enough energy, gravity will affect where trapped atoms drift to and annihilate when the trap is powered down. Observing the z position of a sufficient number of events allows the atom's reaction to gravity to be discerned. This report focuses on the cooling and spectroscopy of $\bar{H}$ with a Lyman-α laser as well as the conceptual design of the detector to be used for the ALPHA-g experiment.

A classical physics order of magnitude estimate demonstrates the need for very cold $\bar{H}$. The thermal energy of an atom in a one degree of freedom trap can be obtained by

$$E = \frac{1}{2}kT$$

If the $\bar{H}$'s momentum is directly upwards from earth, gravity will begin to pull the atom back down when

$$E = \frac{1}{2}kT = mgh$$

The atom will turn around at a height of approximately

$$h \approx 420.7T \tag{1}$$

Therefore, a trap on the order of 1m high must bring $\bar{H}$ to temperatures on the order of millikelvin. ALPHA has achieved evaporative cooling of antiprotons down to temperatures as low as 9K [1] and traps $\bar{H}$ at a temperature on the order of 0.5K [2]. However, the ALPHA-g experiment will likely require laser cooling to perform a 1% measurement of $\bar{g}$. Although, required for ALPHA-g or not, laser cooling will be a significant milestone for future experiments.

H cooling is performed with Lyman-α light. Lyman-α corresponds to the wavelength of the $1s-2p$ transition in H. The idea with laser cooling is to tune the laser to a wavelength slightly longer than Lyman-α. Then, given the one photon process of the $1s_{\frac{1}{2}}-2p_{\frac{3}{2}}$ transition, when the atom is moving towards the beam source, the doppler effect will shift the wavelength to corresponding to Lyman-α and allow excitation. When the photon is absorbed it gives momentum to the atom in the direction perpendicular to the H's momentum hence slowing it down. When the atom relaxes back down to the $1s$ state, a photon is released in a random direction. Therefore, on average, kinetic energy in the axial mode decreases. This method should be able to cool the $\bar{H}$ down to $\sim 20mK$ or colder [3].

Of course, $\bar{H}$ is expected to have the same spectrum as H, thus the same principle should apply. However, experimentally verifying such assumptions is the purpose of ALPHA and a test of CPT symmetry will therefore be made by observing the $1s-2p$ transition in $\bar{H}$. Although the end goal of the Lyman-α project is laser cooling, there is a great deal of adherence and excitement within the collaboration for this experiment as it will be the first ever laser spectroscopy experiment on antimatter.

On another note, once the ALPHA-g experiment is able to attain sufficiently cold $\bar{H}$ in the proposed trap, reconstruction of the location of the annihilation must be achieved. This is another focus of this report. A time projection chamber (TPC) will be used as the detector. A specific gas is contained in the region from $r = 10cm$ to $r = 20cm$ and a detector "mesh", as seen in Figure 2, is wrapped around the outer radius of the apparatus. High energy charged particles following an annihilation create tracks of ionization through the gas. A radial electric field pulls ionized electrons radially outwards to each be detected. Both the hit strip and wire are read out. Given the solution to electron drift through the gas (computed using the software Garfield), the radius of each ionization can be determined by observing the time each electron is detected. By fitting the information from each of these time slices, the position of the annihilation may be reconstructed.

Unfortunately, determining the ϕ and z positions of detections to a sufficient

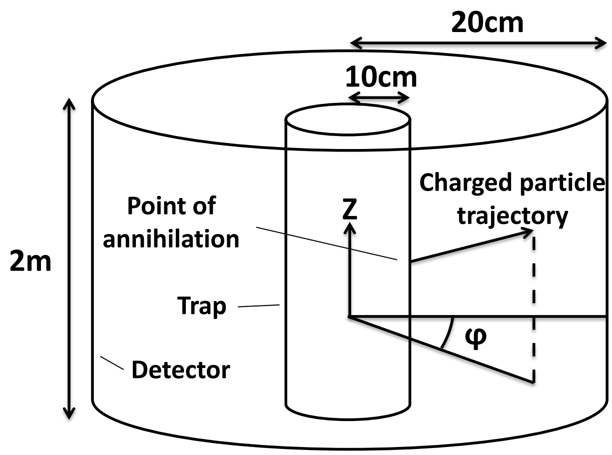

FIG. 1. The antimatter trap and TPC. H-$\bar{H}$ annihilations occur on the inner wall of the trap where high energy charged particles are emitted from.

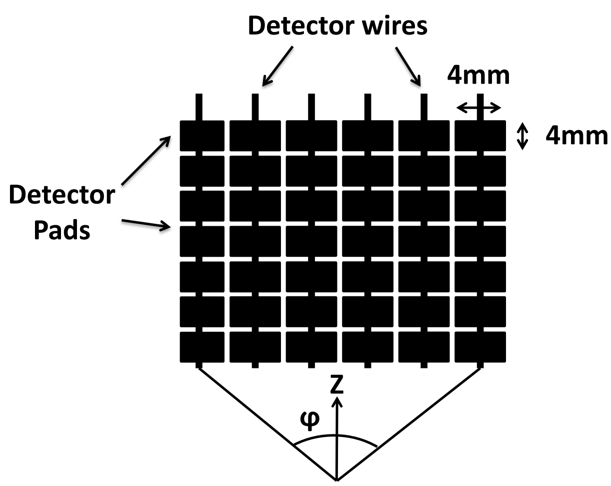

FIG. 2. The original design of the detector.

accuracy proves to be quite difficult. Given the estimated track reconstruction requirement, $4mm$ by $4mm$ strips are required. With 500 strips in z and 300 in ϕ,

$150,000$ strips are required, meaning $150,000$ readout channels. At such a magnitude, air cooling of the electronics is not possible, thus introducing significant design difficulties to an already challenging engineering project. Also, with each channel corresponding to a cost of roughly \$100 along with the purchase of such an amount of wire, funding becomes an additional constraint. Further complications arise from the difficulty of simply fitting the electronics on the apparatus. It is therefore very desirable to reduce this channel count as much as possible without compromising track reconstruction ability.

One solution is to make the strips wider in ϕ as seen in Figure 3. The wires then provide the ϕ information the strips have lost. The issue with this solution is that it introduces something called *ghosting*. Here, ghosting is defined as ambiguity between any two or more detections. Figure 4 depicts ghosting visually. In I, detections occur at the points depicted by the yellow crosses. In II, the corresponding strips and wires are given incremented particle counts depicted by red highlighting. If the detector is now to determine detection positions, event A will clearly have no ambiguity as there is only one possible strip-wire intersection, but ghosting occurs with events B and C. As seen in III, there are 4 possible intersections for only 2 detections and the detector is unable to determine whether detections occurred at 1 and 4 or at 2 and 3 as either events would produce the same readout in the electronics. Since track reconstruction failure occurs due to excessive ghosting, it is greatly sought to quantify and gain as much intuition into this concept as possible.

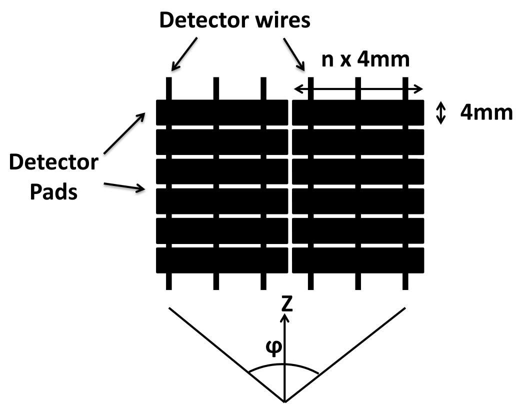

FIG. 3. The newly proposed detector.

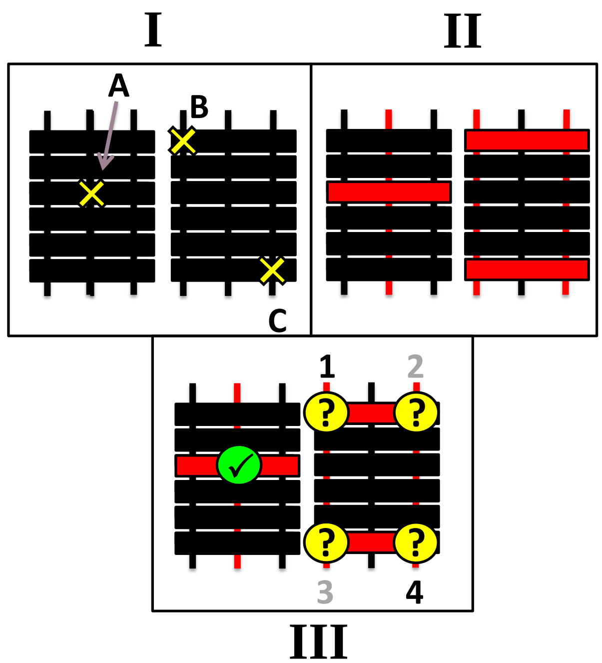

FIG. 4. The mechanism of ghosting. The detector cannot determine whether particles were detected at 1 and 4 or at 2 and 3.

2. GHOSTING IN THE ALPHA-G TIME PROJECTION CHAMBER

I have already spent 4 months on a previous internship at TRIUMF working on a study of ghosting. Part of my time this summer was spent continuing this study. Thus far it has been demonstrated that it should be possible to lower the channel count from the original design of 150,000 to about 10,000 without compromising reconstruction ability. It should be noted that I will continue this study for one of my undergraduate theses meaning that this report is taking place at a midway point in the study.

To start, I was supplied with data produced by Andrea Capra using a simulation in Geant4. As best described by its main website: "Geant4 is a toolkit for the simulation of the passage of particles through matter." Andrea's simulation was of the proposed ALPHA-g apparatus. $\bar{H}$ were annihilated on the inner wall of the trap. High energy charged particles would be emitted from the vertex and I was supplied with the data of where each charged particle exited the drift chamber of the TPC. In practice the detector will gather more data than just this one hit, but here was a good starting point for proving that the techniques I was working on would in fact resolve ghosting. This was a good step up from my original assumption of uniformly distributed tracks. The provided Geant4 data was used in the analyses that follow.

2.1. Increasing Strip Length

The length of detector strips can be increased to reduce the channel count, but ghosting will occur and occur more often. By analytical and simulated means, the plot in Figure 5 was produced.

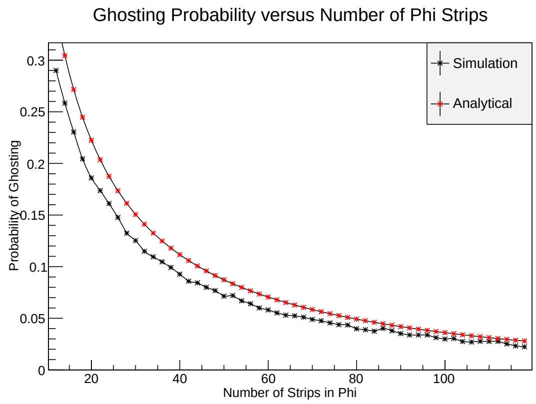

FIG. 5. The probability of ghosting occurring at the end of tracks as calculated by Geant4 data provided by Andrea Capra.

2.2. Technique One: Using Charge Division on Wires

Using charge division on the wires to produce an additional rough estimate of the z coordinate of hits can resolve ghosting a significant portion of the time. The mechanism is depicted in Figure 6. See Figure 7 for a reference of the effect this can have. The interest is in a resolution on the order of an equivalent 10 wire divisions, but it should be noted that a resolution 10 times that may be possible given sufficient means.

2.3. Technique Two: Strip Staggering

It was found that staggering strips as seen in Figure 8 also greatly aids in resolving ghosting. See Figure 9 for a reference of the effect.

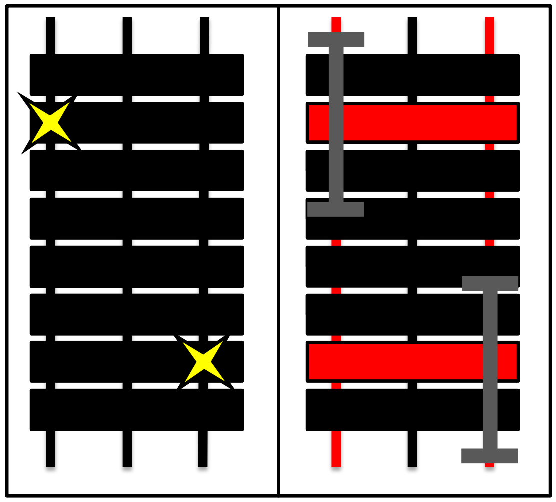

FIG. 6. Now the wires can give a rough estimation of where detections occur on them. See that the two previously allowed ghosted positions can now be dismissed in this case because the wires provide the information that no particle could have been detected on the ghost positions.

2.4. Technique Three: Using Timing Information

Here the analysis begins to consider multiple sections of track. Information from hits along different sections of a track can be used to dismiss ghosts in other time slices. In the TPC there is a 1T uniform magnetic field pointing in the z direction. This is typical as to minimize electron diffusion, but this field also introduces a mechanism that could be exploited to resolve ghosting.

The B-field will cause ionized electrons to bend in ϕ during their drift as shown in the Garfield plot seen in Figure 10. Electrons ionized at more inner radii will bend more given the longer drift region. The result is that all detections resulting from a single track will spread across the detector in ϕ. What the detector will see is shown in Figure 11. As later hits are observed, detections will sweep across in ϕ. If the Lorentz angle is large enough, the case seen in the $t_0 + 3\Delta t$ time slice will be present and this is not a ghost. The reconstruction algorithm previously had 4 possible solutions for

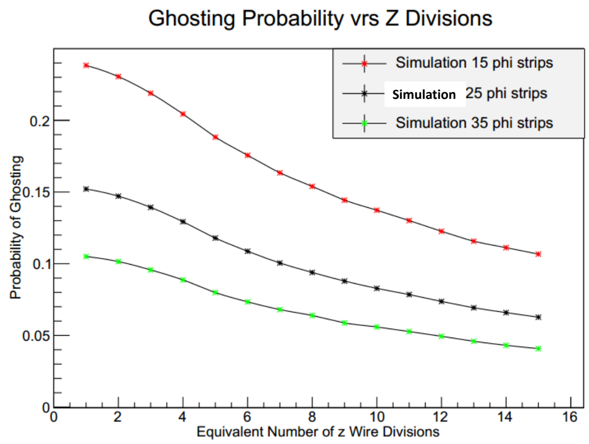

FIG. 7. Plots depicting the effect of introducing z wire resolution are displayed for 15, 25, and 35 strips in ϕ. On the x axis is the equivalent number of wire divisions. For example, 5 wire divisions is 20% position resolution and 10 divisions is 10% position resolution.

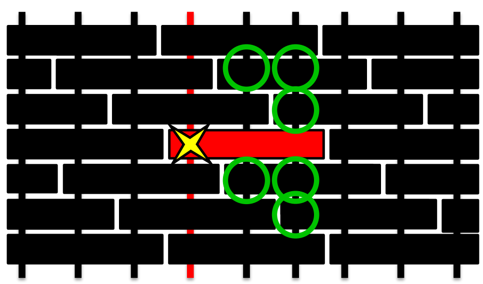

FIG. 8. Ghosting probability is reduced by staggering the strips. Detections at the positions circled in green no longer result in ghosting.

2 tracks, but given a few well defined time slices and the assumption that tracks are continuous in space, ghosted tracks can be dismissed. This allows resolution of all ghosted detections between two tracks.

Assuming two perfectly radial standalone tracks that are not interfered with by

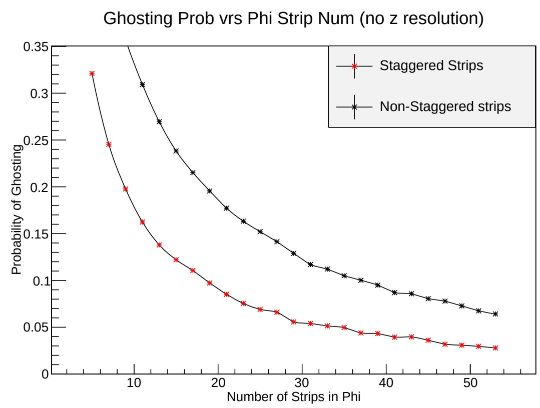

FIG. 9. Ghosting probability versus number of strips in ϕ for the staggered and non-staggered arrangement.

other detections (such as by hits resulting from pair productions in the TPC), it is relatively simple to solve for the probability of the above case occurring and hence estimating the probability of resolving even the tracks containing ghosting.

Observing the case of a ghost occurring, 2 tracks must be within the same $\Delta\phi$, corresponding to one strip length. Assuming that the two tracks are uniformly distributed within $\Delta\phi$, let ϕ_1 and ϕ_2 be their distances from the end of the strip as indicated in Figure 12. See that in order to break ghosting, the Lorentz angle, L, must be large enough such that the leftmost detection will slide over to the next set of strips. Or put another way, the leftmost particle must be placed such that it is a distance less than the Lorentz angle from the end of the strips.

If ϕ_1 and ϕ_2 are uniformly distributed, then their cumulative probability distribution functions are given by

$$P(\phi_1 < L) = P(\phi_2 < L) = \frac{L}{\Delta\phi}$$

and thus

$$P(\phi_1 > L) = P(\phi_2 > L) = 1 - \frac{L}{\Delta\phi}$$

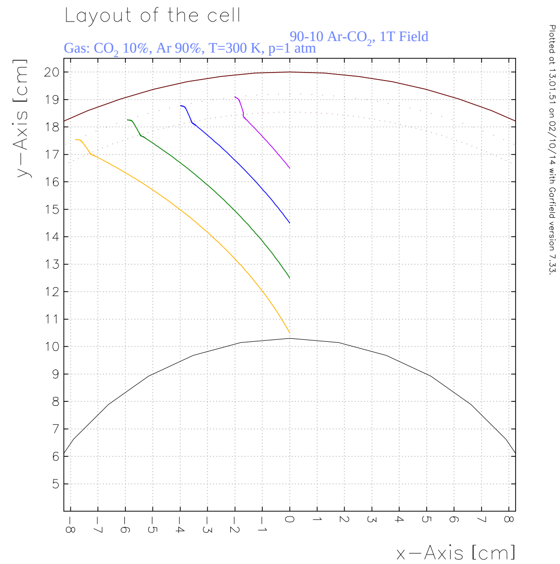

FIG. 10. A plot of electron drift in the TPC as provided by Phillip Lu and Robert Henderson of TRIUMF. This plot was made with Garfield. Different colored tracks correspond to the paths that electrons will take in the drift chamber given ionizations at different radii.

therefore

$$P(\phi_1 > L \cap \phi_2 > L) = (1 - \frac{L}{\Delta\phi})^2$$

and see that the compliment of this is the probability that either ϕ_1 *or* ϕ_2 is less than L, ie

$$P(\phi_1 < L \cup \phi_2 < L) = 1 - (1 - \frac{L}{\Delta\phi})^2$$

where

$$\Delta\phi = \frac{2\pi}{\#\ of\ \phi\ strips}$$

The probability of breaking a ghost for radial tracks using timing information is

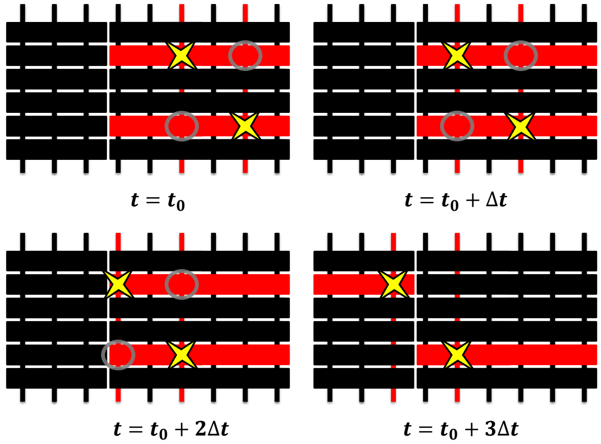

FIG. 11. As later time slices come in (a later time slice means ionization occurred at a more inner radii which means a longer drift region for the electron), detections will sweep across the detector in ϕ. As seen in the time slice $t_0 + 3\Delta t$, ghosting can be broken.

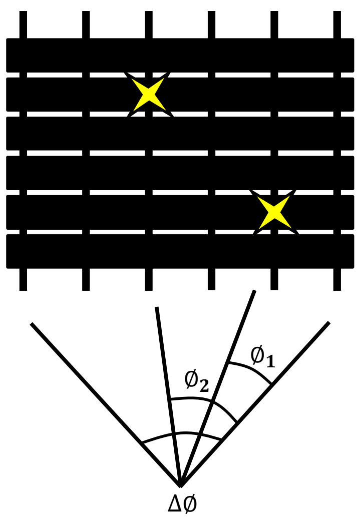

FIG. 12.

thus given by

$$P_t = 1 - (1 - \frac{L}{\Delta\phi})^2 \tag{2}$$

P_t is plotted versus the number of strips in ϕ for two of the gases considered for the drift chamber in Figures 14 and 13.

Adding isobutane to the gas acts as a way to tune the Lorentz angle to whatever

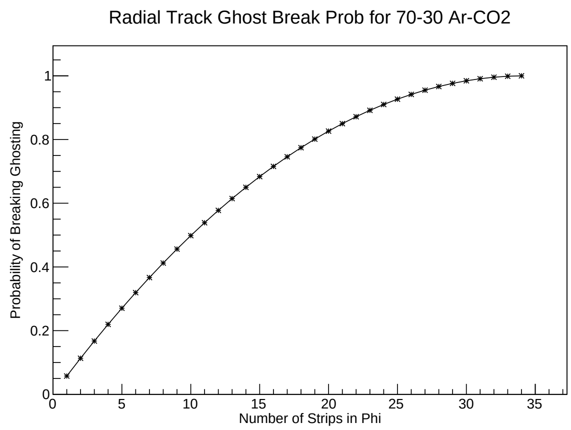

FIG. 13. The probability of breaking ghosting for two standalone radial tracks for the 30% CO_2 70% Ar gas which has a Lorentz angle of 10.5 degrees.

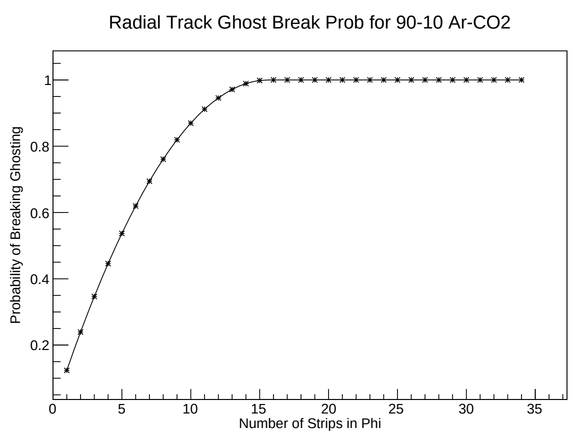

FIG. 14. The probability of breaking ghosting for two standalone radial tracks for the 10% CO_2 90% Ar gas which has a Lorentz angle of 23 degrees.

is desired, which leaves L as a design parameter. A larger Lorentz angle means ghosting is easier to break and a smaller Lorentz angle allows easier prototyping at TRIUMF given that TRIUMF does not have a large magnet to test with.

2.5. Further Development

I began to work with and modify Andrea Capra's simulation in order to analyze data from all portions of tracks rather than just the outermost hit. Figure 15 displays an annihilation event in the proposed $\bar{H}$ trap. Note that photon tracks are not displayed.

In order to easily observe the effect of using a gas with a differnt Lorentz angle, a

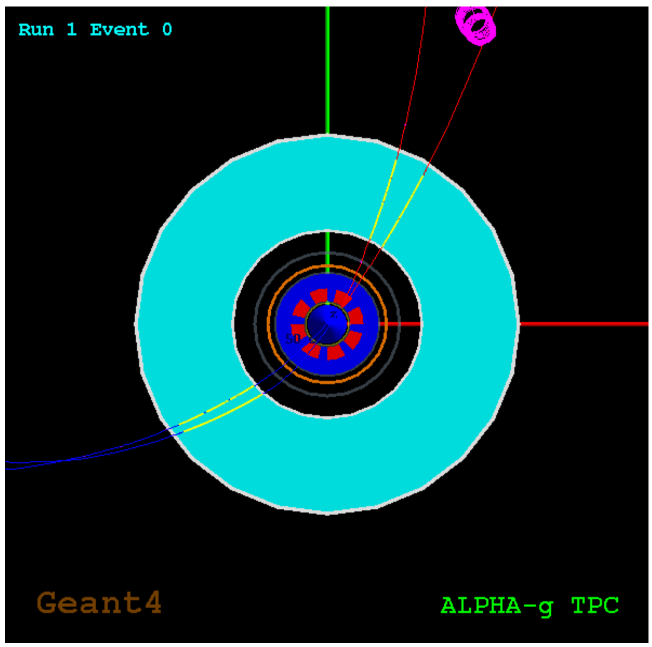

FIG. 15. An image produced by Andrea Capra's Geant4 simulation. This is an example of ghosting. Red tracks are $\pi^{+}s$, blue tracks are $\pi^{-}s$.

first order calculation to simulate electron drift can be performed using Equation 3.

$$\phi_{detector} = \phi_{hit} + L \cdot \frac{r_{hit} - r_{inner}}{r_{outer} - r_{inner}} \tag{3}$$

$\phi_{detector}$ is the coordinate of where ionized electrons will drift to. ϕ_{hit} is the coordinate of the ionization. r_{hit} is radius of the ionization and r_{inner} and r_{outer} are the inner and outer dimensions of the TPC.

A data structure was written in Geant4 for storing hits in the TPC. In each event, the program takes a hit position (corresponding to an ionization) of each emitted pion 20 times through its track through the drift region (corresponding to 20 time slices). From each of these points, electron drift is simulated and the hit pad, wire, and section of wire is stored. Then, the hits in each time slice are observed for ghosting and that data can be written to file for analysis in Root. My thesis will continue at this point and will use this data to more thoroughly analyze ghosting and to create better metrics for determining when a detector design is sufficient or not.

3. LYMAN-α LASER IMAGING

The other focus of this term was on the imaging of ALPHA's Lyman-α laser. ALPHA traps antimatter using its magnetic dipole. When Lyman-α light is shone on the trapped $\bar{H}$ there is a possibility of the transition from the $1s$ to $2p$ state. If there is a spin flip during the transition, the $\bar{H}$ will enter an untrappable state and will annihilate on the wall of the trap shortly after. The detector will see this signal, indicating that the $1s-2p$ transition was observed. Performing this experiment and confirming the symmetry between H and $\bar{H}$ was the goal during my time at CERN.

Due to the limited amount of beam time we were given this summer, work needed to be swift. As time was running out, it seemed as though we would not get the laser through trap, but on the very last day everything seemed to come together. There was not enough time that night to take enough data to publish, but we did get to perform a mock experiment. Despite the 24 hour shift, it was an honor be present for such an event led by the Canadian members of the ALPHA collaboration. A bit of memorabilia for the ALPHA control room is seen in Figure 16.

My mini project with the Lyman-α experiment was to monitor various parame-

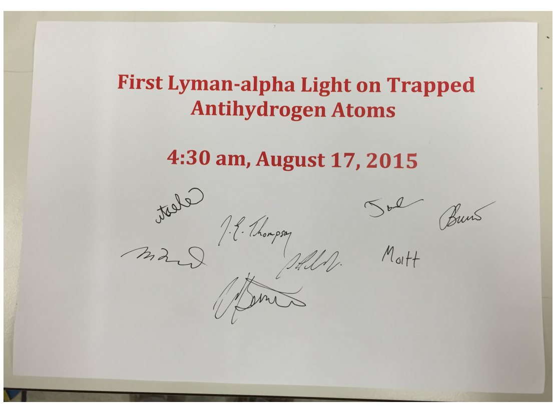

a) b)

FIG. 16. a) Some history for ALPHA. b) Given the unexpectedness of the success, nobody thought to bring proper celebration juice. As it turned out though, Makoto had this kicking around for a 9am celebration after a long night.

ters of the beam at 10Hz. The laser emitted 10ns bursts every 100ms. After passing through the antimatter trap, the pulse would strike a microchannel plate (MCP). Our MCP would convert and amplify Lyman-α light from vacuum into a photoluminescent signal on a phosphor plate. The result was a $\sim 2ms$ signal composed of visible light. My project was characterizing the MCP output with a very high sensitivity CCD camera controlled by LabVIEW.

The required output was the x,y position of the beam center, a 2D characterization of beam width (FWHM), the total energy of pulses, an image running average of the beam, and a real time camera display. Various conveniences for data acquisition and storage were also required. This all needed to be performed at 10Hz without storing images to disk given that the experiment is to be run for hours and disk space would fill completely in just a few minutes given the acquisition rate. It was desired to obtain each parameter for a $\sim$1-2s average that missed no more than 5% of the pulses. It was also desired to obtain the total energy of each individual pulse, but as it turned out, our hardware was not ideal for this functionality. In theory, this information was attainable, but it would need to be extracted using an unconventional method and would also be *very* difficult to accomplish. My setup had all required functionality except for this.

3.1. Hardware

After the MCP, the CCD camera would stream the images it took to a PIXCI SV5 Frame Grabber PCI card on a desktop. Then, using the XCLIB library, LabVIEW would talk to the frame grabber to extract images of the MCP and analyze them. This setup was purchased as a package from a third party as MCP's can be very expensive and a very good deal was found in this case. The fallback was zero support from the camera manufacturer and more or less zero documentation on the hardware. This hence made up a fair portion of the project as it was left up to me to figure out via experimentation all functionality. I then needed to determine how the setup could be used for our purpose.

One discovery was that the CCD camera exposes alternate fields (images containing only every second row of pixels) each at 60Hz according to the camera's own internal clock and could not be synced to an external clock. This means that one cannot control nor know when the camera's exposures occur. A pulse could therefore take place in two different exposures meaning that the two images would need to be added if a proper intensity integral is to be performed on every pulse. With some work, this type of shot-to-shot capture may be possible, but further complications that are explained later made this path undesirable. For the parameters required of the image average, given that each exposure is 17ms and each pulse is $\sim 2ms$, it is unlikely that exposures not containing all of a pulse will affect the average significantly. The required parameters on the beam average were deemed to therefore be attainable with sufficient.

It was also discovered that exposures from the camera are continuously streamed one line at a time to an image buffer. One can only take a snapshot of this buffer at a given point in time. Unfortunately, this snapshot will always contain some lines from one exposure and some from the preceding exposure. The result is expressed in Figure 17. These images were obtained by accessing the camera's buffer at 180Hz. Notice that only a few horizontal lines of the image are updated from a) to b) and from b) to c). An image from a single exposure can be obtained, but this function does not return fast enough to extract at 10Hz.

The solution was to access the image buffer faster than 60Hz and use LabVIEW

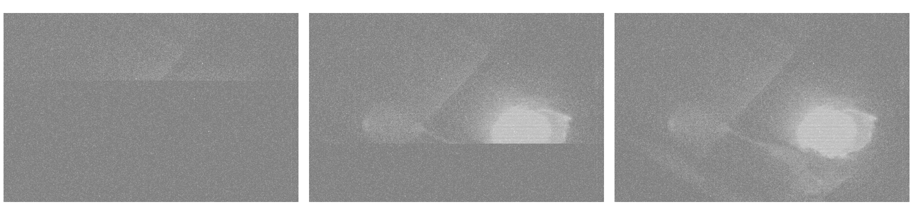

a) b) c)

FIG. 17.

to determine which of the extracted images to keep for analysis. Otherwise, one risks accepting and analyzing a cutoff image such as that seen in b). This reality makes shot-to-shot capture significantly more difficult with the given hardware. Not only would the analysis need to add certain exposures together, but also obtain and pinpoint which buffer extractions contain the correct lines corresponding to the two different exposures of interest. This would all have to be performed using image processing in LabVIEW. Although possible, the proper way to achieve shot-to-shot capture is with a camera that exposes on a trigger. Such a camera may cost on the order of $50,000 however and such funding lacks the necessary justification. I hence decided not to pursue shot-to-shot capture.

One other confirmation needed was that the pixel values of images scaled linearly with energy deposited by light. This was checked by pulsing an LED on and off and varying the on time (pulse-width modulation). An intensity integral can then be performed over the image. The results are seen in Figure 18 and it was indeed confirmed that pixel data scaled linearly with energy deposit.

3.2. LabVIEW

The functionality of the hardware defined how the image processing would be undertaken. Figure 19 shows the front panel of the data acquisition program. It makes more sense for the following part of this report to be more along the lines of a guide to using my software.

1. A "spot finder" is used on each image extracted from the camera's buffer to select which contain the beam image and are to be used for analysis. The spot finder settings must be set by the user. "Camera Images and Beam Finder" is the image used to tune the program's spot finder as well as have a reference of what the camera sees pre-processing. For best performance it should be tuned as described in 5 - Beam Finder Settings.

2. Image Processing Settings. Turning on "Beam Tracking" will have "Camera

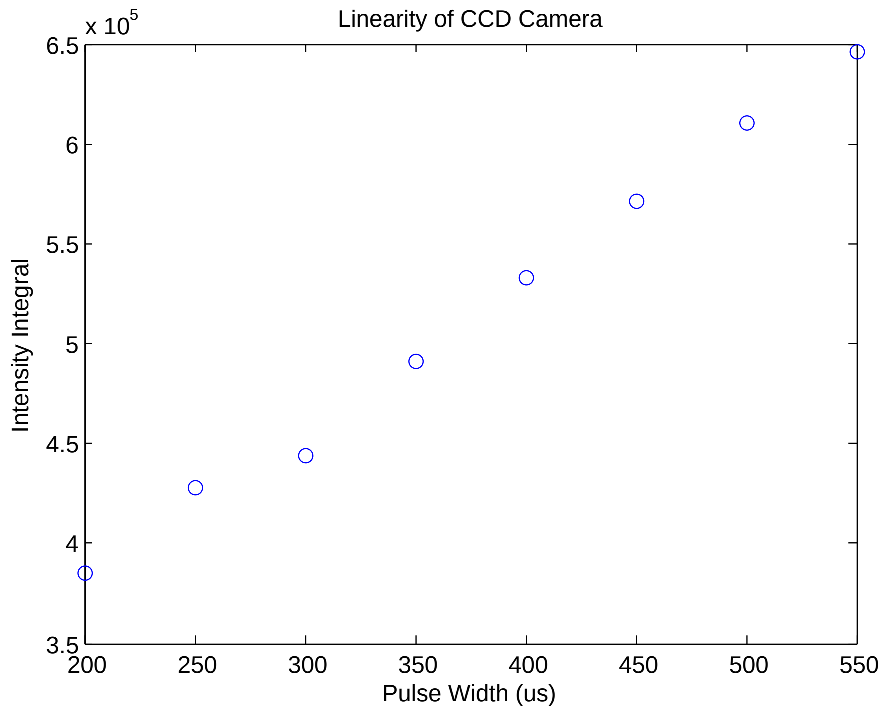

FIG. 18.

Images and Beam Finder" display only images where the beam was detected. Turning on "Fit Beam" will perform Gaussian fits to every beam image rather than just on the averaged image. The loop rate sets the upper bound rate at which the camera's buffer data is accessed (if settings are not optimized, the program may not be able to run as fast as the set speed).

3. Data Logging Settings. Turning on "Save Data" will save the averaged image, the required analysis of the averaged image (as previously described), and all pictures with the beam in it. If "Fit Data" is also turned on then the program will save the analysis of each individual image as well, although there is no guarantee that this shot-to-shot capture will be reliable due to exposures possibly not capturing all of a pulse.

4. The running average constant is set to 100 by default. This means that for each

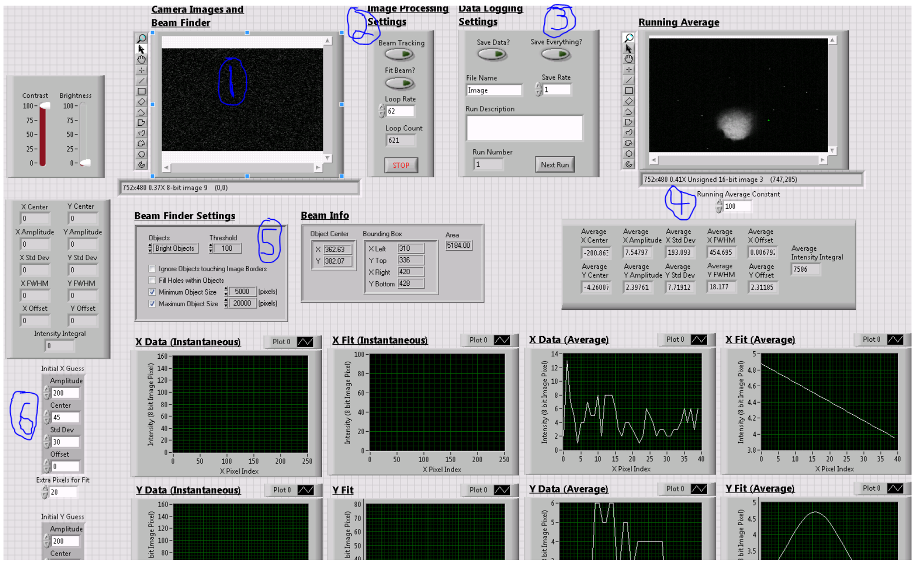

FIG. 19.

new image captured, the previous average is multiplied by 99 and added to the new image. This sum is then divided by 100. The images where the spot finder sees the beam is found are the images averaged.

5. The beam finder settings must be chosen appropriately to ensure the analysis is correct. Also, settings that are not optimized will cause the loop rate to be slow which may result in missing a significant number of laser pulses. Turning on “Beam Trackin” will allow the user to see only the beams that are detected as a reference.

6. The initial guesses for the Gaussian fit parameters. These must be tuned decently to assure that the fitting algorithm does not get stuck in a local max.

4. SETTING UP FOR THE EXPERIMENT

Once the Lyman-α beam was sent to the apparatus, the first step was to image it before sending it through the trap. This was also important since the beam profile had never been seen before which was especially important for the development of the fitting algorithm. Figure 20 shows the first image taken of the beam. Although very faint, it was noted that the profile was more or less circular.

After some manipulation of the system's optical setup, the beam was ready to

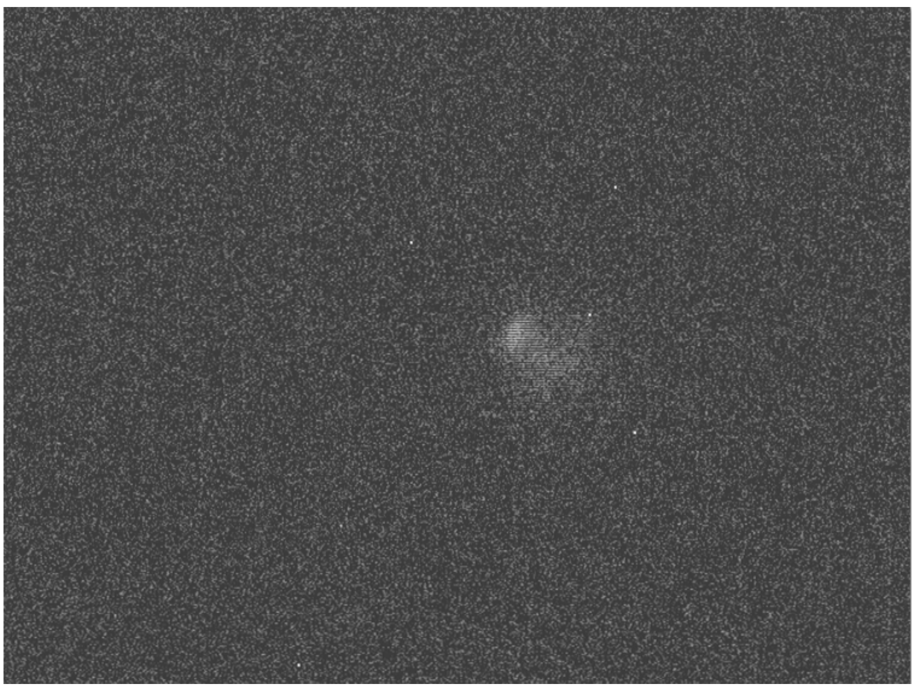

FIG. 20.

imaged again. Seen in Figure 21 a) is a 20 image average of the beam. In b) are Gaussian fits to the pixel data. At this point it was noted that even with averaging, a Gaussian profile was not observed. This prompted a new fitting algorithm to attain the beam width as the FWHM given in Figure 21 b) was not accurate.

Regardless of the fitting accuracy, the beam width was far too large to pass through the trap so, among other things, a colinear geometry of lenses was tried to columnate the beam. The plots seen in Figure 22 were then produced with a

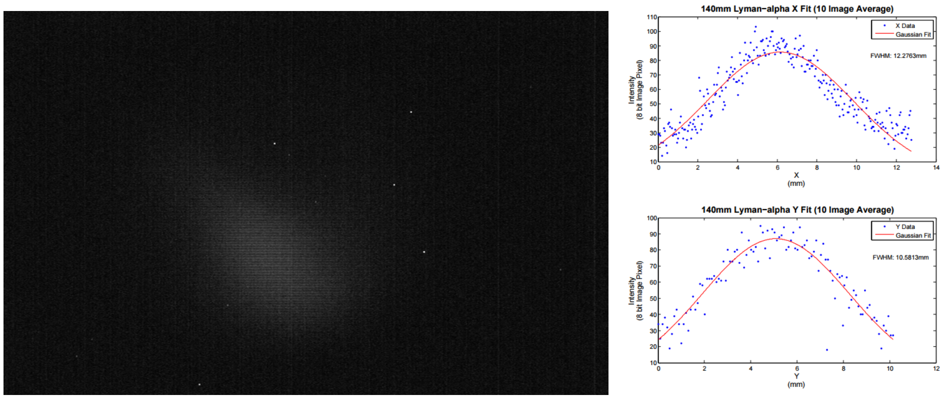

FIG. 21.

more appropriate fitting algorithm. Figure 23 depicts a summary of the beam widths achieved with different lens separations.

A lens separation of 205mm was found to give the smallest beam width and was thus selected to proceed. The beam was then passed through the trap and detected with a PMT. See Figure 24 for the signal obtained with the PMT. The signal was mostly from 365nm light, but there was still clear indication that Lyman-α light was present as well. This prompted us to proceed with an experiment on $\bar{H}$ that night.

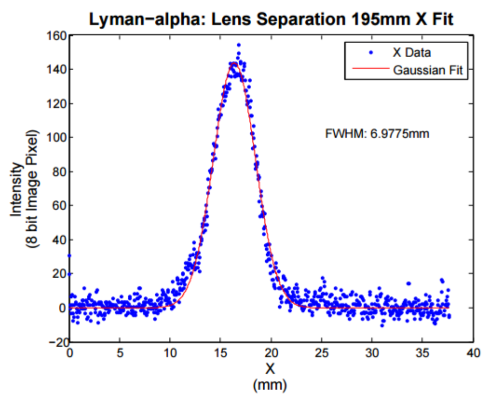

a)

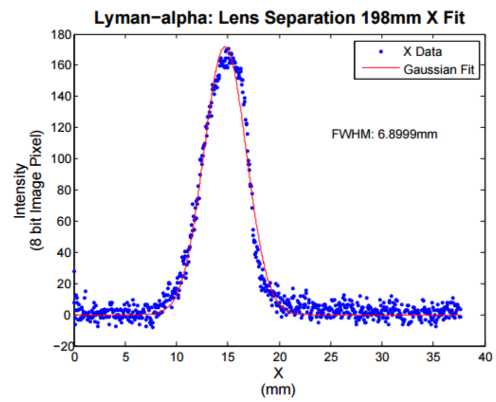

b)

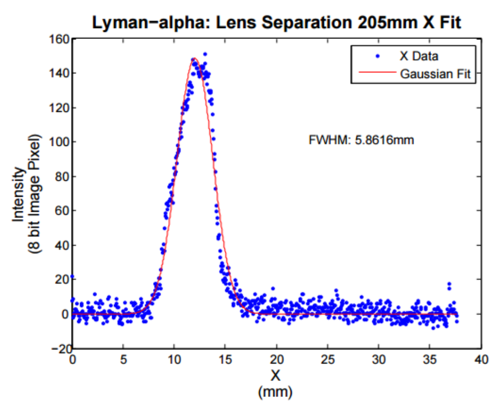

c)

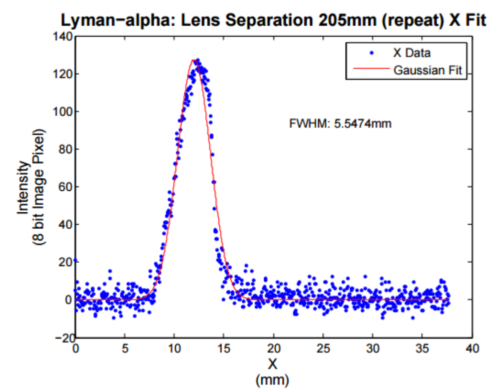

d)

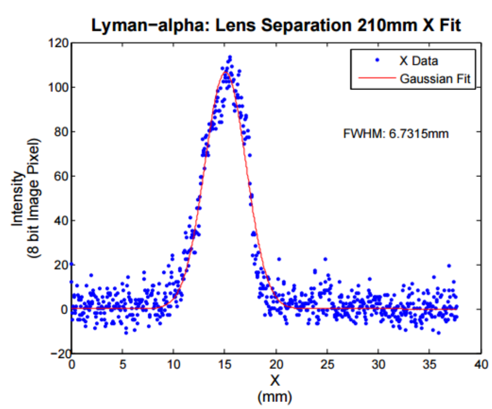

e)

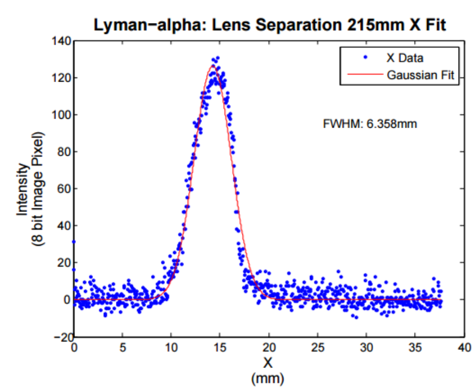

f)

FIG. 22.

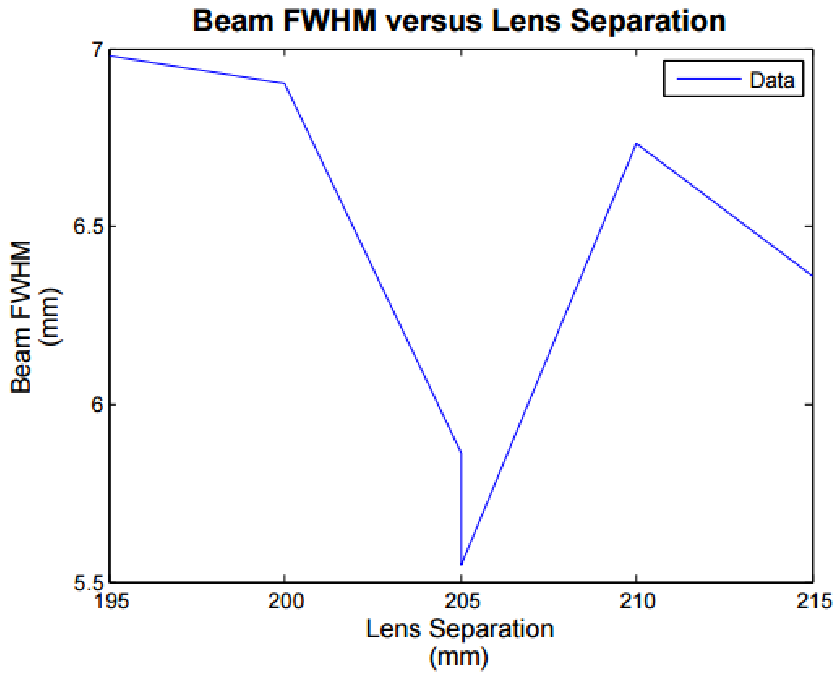
Beam FWHM versus Lens Separation
Data
Beam FWHM
(mm)
Lens Separation
(mm)
7
6.5
6
5.5
195
200
205
210
215

FIG. 23.

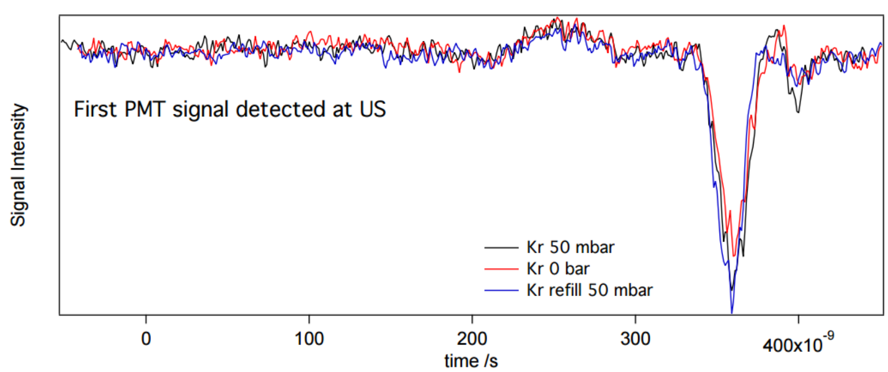
First PMT signal detected at US
Kr 50 mbar
Kr 0 bar
Kr refill 50 mbar
Signal Intensity
time /s
0
100
200
300
400x10^-9

FIG. 24.

5. SUMMARY

Work performed for two of ALPHA's experiments were presented. The first experiment being ALPHA-g, where the gravitational reaction of $\bar{H}$ is sought. The second experiment being the Lyman-α experiment where the $1s-2p$ transition in $\bar{H}$ is under observation for CPT symmetry with H. Further motivation behind the Lyman-α setup is to be able to laser cool $\bar{H}$ which will likely be necessary for the ALPHA-g experiment as well as other future experiments. The ALPHA-g work performed consisted of a study of ghosting in the ALPHA-g time projection chamber using Geant4 and Root. The work with Lyman-α involved hardware and LabVIEW development for the imaging of ALPHA's Lyman-α laser.

The groundwork for a thorough study of the ALPHA-g time projection chamber in Geant4 has now been completed. Given a project of such a scale as ALPHA-g, a very thorough proof of concept is needed before proceeding. For this part of the experiment, at this stage, it is now just a matter of analyzing Geant4 data which I will continue on as an undergraduate thesis.

The Lyman-α imaging setup is at the point of a standalone unit capable of most of the functionality desired. The setup will accurately obtain images of the beam (which is pulsed at 10Hz), it will find the beam width, position, and energy deposit. This data can be written to file along with specific (relevant) images. A running average of the beam image is also displayed and analyzed the same way. The functionality not accomplished was perfect shot-to-shot capture to obtain the energy deposit of individual laser pulses. Unfortunately, due to hardware and software restrictions, missing part of the energy deposit of the odd pulse is inevitable. Obtaining this functionality will hence not be pursued as a proper camera would be very expensive. Nonetheless, the setup works well when averaging images and was sufficient to setup for a mock spectroscopy experiment on $\bar{H}$.

[1] Andresen, Gorm Bruun *Evaporative cooling of antiprotons and efforts to trap antihydrogen*. Diss. Aarhus University, Aarhus, 2010. Aarhus University Department of Physics and Astronomy PhD Theses. Wed. 2 Sept 2015.

[2] Amole, C., G.b. Andresen, M.d. Ashkezari, M. Baquero-Ruiz, W. Bertsche, P.d. Bowe, E. Butler, A. Capra, P.t. Carpenter, C.l. Cesar, S. Chapman, M. Charlton, A. Deller, S. Eriksson, J. Escallier, J. Fajans, T. Friesen, M.c. Fujiwara, D.r. Gill, A. Gutierrez, J.s. Hangst, W.n. Hardy, R.s. Hayano, M.e. Hayden, A.j. Humphries, J.l. Hurt, R. Hydomako, C.a. Isaac, M.j. Jenkins, S. Jonsell, L.v. Jrgensen, S.j. Kerrigan, L. Kurchaninov, N. Madsen, A. Marone, J.t.k. Mckenna, S. Menary, P. Nolan, K. Olchanski, A. Olin, B. Parker, A. Povilus, P. Pusa, F. Robicheaux, E. Sarid, D. Seddon, S. Seif El Nasr, D.m. Silveira, C. So, J.w. Storey, R.i. Thompson, J. Thornhill, D. Wells, D.p. Van Der Werf, J.s. Wurtele, and Y. Yamazaki. "The ALPHA Antihydrogen Trapping Apparatus." *Nuclear Instruments and Methods in Physics Research Section A: Accelerators, Spectrometers, Detectors and Associated Equipment* 735 (2014): 319-40. *Science Direct*. Web. 21 Sept. 2015.

[3] Donnan, P H, M C Fujiwara, and F. Robicheaux. "A Proposal for Laser Cooling Antihydrogen Atoms." *J. Phys. B: At. Mol. Opt. Phys. Journal of Physics B: Atomic, Molecular and Optical Physics* (2013): 025302. Print